Impact of the selected boundary layer schemes and enhanced horizontal resolution on the Weather Research and Forecasting model performance on James Ross Island, Antarctic Peninsula

Michael Matějka[*], Kamil Láska[**]

Department of Geography, Faculty of Science, Masaryk University, Kotlářská 2, 611 37 Brno, Czech Republic

Abstract

The output of the various Weather Research and Forecasting (WRF) model configurations was compared with ground-based observations in the northern part of James Ross Island, Antarctic Peninsula. In this region, a network of automatic weather stations deployed at ice-free sites (as well as small glaciers) is operated by the Czech Antarctic Research Programme. Data from these stations provide a unique opportunity to evaluate the WRF model in a complex terrain of James Ross Island. The model was forced by the ERA5 reanalysis data and the University of Bremen sea ice data. The model configurations include a novel Three-Dimensional Scale-Adaptive Turbulent Kinetic Energy (3D TKE) planetary boundary layer scheme and a more traditional Quasi-Normal Scale Elimination (QNSE) scheme. Impact of model horizontal resolution was evaluated by running simulations in both 700 m and 300 m. The validation period, 25 May 2019 to 12 June 2019, was selected to cover different stratification regimes of air temperature and a significant snowfall event. Air temperature was simulated well except for strong low-level inversions. These inversions occurred in 44% of all cases and contributed to a higher mean bias (2.0–2.9°C) at low-elevation sites than at high altitude sites (0.2–0.6°C). The selection of the 3D TKE scheme led to improvement at low-elevation sites; at high altitude sites, the differences between model configurations were rather small. The best performance in wind speed simulation was achieved with the combination of the 3D TKE scheme and 300 m model resolution. The most important improvement was decrease of bias at a coastal Mendel Station from 3.5 $m \cdot s^{-1}$ with the QNSE scheme on the 700 m grid to 1.2 $m \cdot s^{-1}$ with the 3D TKE scheme on the 300 m grid. The WRF model was also proven to simulate a large snowfall event with a good correspondence with the observed snow height.

Key words: polar meteorology, numerical simulation, WRF model, air temperature, snow cover, wind speed, Antarctic Peninsula

DOI: 10.5817/CPR2022-1-2

Received June 7, 2022, *accepted* July 16, 2022.

[*]Corresponding author: Matějka[*] <matejkamichael@mail.muni.cz>, Láska[**] <laska@sci.muni.cz>

Acknowledgements: The authors acknowledge the crew of Johann Gregor Mendel station for their fieldwork support and help with the maintenance of the meteorological stations. Access to the CERIT-SC computing and storage facilities provided by the CERIT-SC Center, under the program 'Projects of Large Research, Development, and Innovations Infrastructures' (CERIT Scientific Cloud LM2015085), is greatly appreciated. We are also grateful for the useful and constructive comments from two anonymous reviewers, which substantially improved this study. The authors are grateful to EMS Brno (Czech Republic) for the development and long-term support of research-grade devices and meteorological systems.

Funding: This work was supported by the Czech Science Foundation (Project GC20-20240S); the Czech Antarctic Research Programme 2022 (VAN 2022), funded by the Ministry of Education, Youth and Sports of the Czech Republic and a project of Masaryk University (MUNI/A/1393/2021).

List of Abbreviations: 3D TKE = Three-Dimensional Scale-Adaptive Turbulent Kinetic Energy, AP = Antarctic Peninsula, AWS = automatic weather station, ERA5 = ECMWF Reanalysis v5, PBL = planetary boundary layer, RMSE = root mean square error, SWE = snow water equivalent, QNSE = Quasi-Normal Scale Elimination, WRF = Weather Research and Forecasting

Introduction

Antarctic Peninsula (AP) is one of the regions with the highest climate variability in Antarctica. After rapid warming in the late twentieth century, a pronounced cooling was observed in the early twenty-first century (Turner et al. 2016). Due to relatively high summer temperatures, regional climate fluctuations could have a strong impact on local cryosphere (*e.g.* Davies et al. 2012, Jonsell et al. 2012, Oliva et al. 2017). An important factor for temperature variability and glacier melt intensity on the eastern side of the AP is the change in frequency of foehn winds (Cape et al. 2015). Complex interactions between the atmosphere and the cryosphere constitute a crucial research topic due to ongoing global climate change connected with enhanced glacier melt (IPCC 2019). However, *in situ* observations in the AP region are limited due to its remoteness and harsh polar conditions. In recent decades, numerical models of the atmosphere became an important tool in polar meteorology and climatology (*i.e.* for reconstructions or projections of future climate variability and processes). They were also proven useful in precipitation and snow cover modelling (Monaghan et al. 2018) and in simulating snow transport by wind (Gallée et al. 2013). The Weather Research and Forecasting (WRF) model was successfully applied in Antarctica (*e.g.* Tastula et al. 2011, Turton et al. 2017, Zhang and Zhang 2018), Svalbard (Aas et al. 2015, 2016; Láska et al. 2017) and Greenland (Turton et al. 2019). The WRF model was already run over northern James Ross Island at 700 m horizontal resolution with several traditional planetary boundary layer (PBL) schemes (Matějka et al. 2021). The selected PBL schemes led to good model performance while winter air temperature inversions and wind speed at low-elevation sites were identified as the main challenges. Here, we present new results based on a comparison of a traditional Quasi-Normal Scale Elimination (QNSE) boundary layer scheme and a new Three-Dimensional Scale-Adaptive Turbulent Kinetic Energy (3D TKE) scheme that is supposed to be more suitable for model resolution in the several-hundreds-of-meters order. Furthermore, the potential benefit of increasing model resolution from 700 m to 300 m was assessed. The impact of the described changes on the model's ability to predict air temperature, wind speed, fresh snow height, and snow water equivalent (SWE) during a significant snowfall was evaluated.

Methods

Automatic weather stations observations

Data from five automatic weather stations (AWS) located in the northern part of the Ulu Peninsula, James Ross Island, AP, provided an observational background for model validation (Fig. 1). This AWS network covered an altitudinal range of 10 – 539 m and included both ice-free sites and selected Ulu Peninsula glaciers. Air temperature was observed by the EMS33 temperature sensor (EMS, Brno, the Czech Re-

public), and wind speed was monitored by a Young 05305 anemometer (Young, Traverse City, United States). Snow height was measured by a sonic distance sensor (Judd Communications, Salt Lake City, United States). Air temperature was available every hour, wind speed was recorded as 30-min means and the snow height sensor provided data with 2-h resolution. Geographical coordinates of the AWS locations and their instrumentations are provided in Table 1 and Table 2.

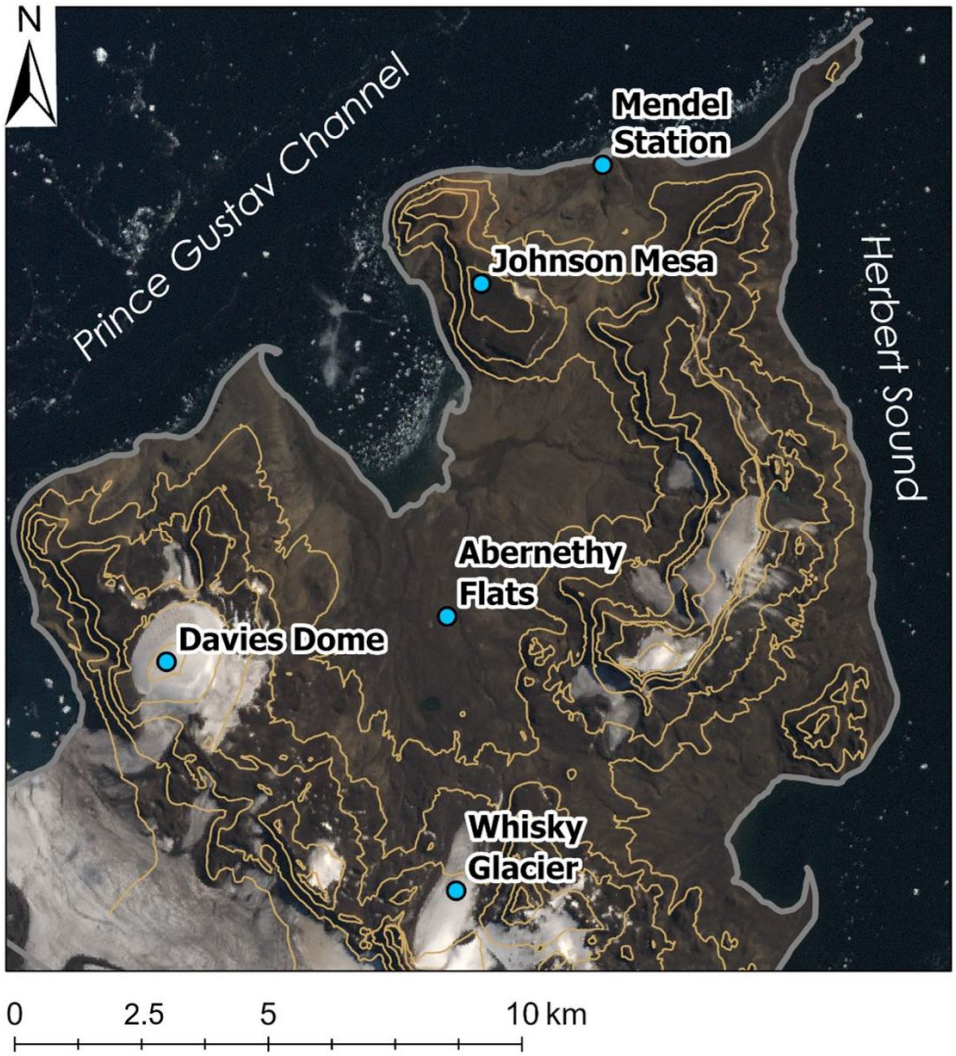

Fig. 1. AWS locations (blue circles) on the Ulu Peninsula, James Ross Island. The background map is created from the Landsat Imagery Mosaic of Antarctica (Bindschadler et al. 2008) and the Czech Geological Survey elevation data (Czech Geological Survey 2009).

AWS location	*Latitude (°)*	*Longitude (°)*	*Altitude (m)*	*WRF altitude (m)*	*Land cover*
Abernethy Flats	-63.8814	-57.9482	41	65/64	*Bare ground*
Davies Dome	-63.8887	-58.0611	539	514/539	*Glacier*
Johnson Mesa	-63.8223	-57.9326	340	261/349	*Bare ground*
Mendel Station	-63.8016	-57.8832	10	10/27	*Bare ground*
Whisky Glacier	-63.9300	-57.9461	326	330/348	*Glacier*

Table 1. Geographical coordinates, in situ and the WRF model altitude and land cover type of the Ulu Peninsula AWS locations. The WRF altitude is given as the altitude of the closest model grid point at 700 m/300 m resolution.

AWS location	*Air temperature*	*Wind speed*	*Snow height*
Abernethy Flats	✓		
Davies Dome	✓	✓	
Johnson Mesa	✓		✓
Mendel Station	✓	✓	✓
Whisky Glacier	✓		

Table 2. Meteorological parameters observed at Ulu Peninsula AWS locations.

The WRF model

The WRF model is an open-source, state-of-the-art weather prediction system. It features advanced numerical schemes for atmospheric dynamics and multiple parameterisations of physical processes (*e. g.* cloud microphysics, radiation and land surface-atmosphere interactions) (Wang et al. 2021). The model has been used successfully in many atmospheric research studies in Antarctica (*e.g.* Steinhoff et al. 2013, Turton et al. 2017) and in Antarctic weather prediction (Antarctic Mesoscale Prediction System; for more details, *see* [1]).

In this study, the model was run in version 4.3, which was released in May 2021. This version includes a new 3D TKE model (Zhang et al. 2018) as a boundary layer scheme option. The 3D TKE scheme was developed to overcome the limitations of traditional boundary layer schemes in model grid resolutions significantly below 1 km (Shin and Dudhia 2016). The 3D TKE model was compared with a traditional QNSE boundary layer scheme (Sukoriansky et al. 2005). Potential benefits from enhanced horizontal resolution were assessed by running the model in two sub-kilometer grid resolutions (700 m and 300 m). Shortwave and longwave radiation fluxes in the model were computed by the Rapid Radiative Transfer Model for Global Circulation Models (Iacono et al. 2008); the Thompson scheme (Thompson et al. 2008) was responsible for cloud microphysics; and the NoahMP scheme (Niu et al. 2011) was selected as the land surface model for computing atmosphere-land interactions. This scheme supports multilayer snowpack and snow compaction by multiple physical processes but does not support snow redistribution by wind. Convection, if any should occur, was simulated explicitly. The 3D TKE scheme was run with the Mellor-Yamada-Nakanishi-Niino surface layer scheme, and the QNSE

boundary layer scheme relied on an eponymous surface layer option.

The validation period lasted from 25 May 2019 01 UTC to 12 June 2019 00 UTC. However, simulations were initiated nine days before the validation period to allow development of local atmospheric processes (Warner 2009). This period was selected to capture contrasting meteorological conditions: a strong temperature inversion, slightly stable or neutral temperature stratification and a significant snowfall event. The impact of strong low-level temperature inversion on air temperature and wind speed accuracy was assessed by computing model bias in four subperiods, two of which included a very strong air temperature inversion with a temperature contrast of more than 10°C between coastal Mendel Station and nearby Johnson Mesa, which is 340 m above sea level.

The WRF model simulation design included three nested domains for 700 m runs and four nested domains for 300 m runs. In the vertical coordinate, the model worked with 65 eta levels. Adaptive time step was chosen to reach reasonable computational cost while keeping numerical schemes in the model stable. The ERA5 reanalysis (Hersbach et al. 2020) provided atmospheric initial and boundary conditions for the WRF model. The University in Bremen sea ice dataset (Spreen et al. 2008) was a source of detailed sea ice concentration input. Mean sea ice depth was set to 1.2 m following analysis of Kern et al. (2016). Model terrain height was derived from the Reference Elevation Model of Antarctica (Howat et al. 2019). Land cover categories of individual model grid points (sea, ice/snow and bare ground) were based on the SCAR Antarctic Digital Database (British Antarctic Survey, 2019) and Czech Geological Survey data (2009). Initial model snow cover and snow density adjustments for Antarctica were made in the same manner as in Matějka et al. (2021).

The accuracy of the model output was assessed with three standard validation statistics: Pearson correlation coefficient (r_{xy}), bias (positive if the model predicted a higher value than was observed) and the root mean square error (RMSE). Validation statistics were not computed for snow height because relative snow height was used for comparison (*i.e.* existing snow height at the beginning of the validation period was subtracted from the evaluated time series). Note that modelled wind speed at Davies Dome AWS was corrected from model height (10 m) to observation height (2 m) by a logarithmic function (Johnson 1999). The conversion formula was

$$U_2 = U_{10} * \frac{\ln\left(\frac{2}{0.002}\right)}{\ln\left(\frac{10}{0.002}\right)} \qquad Eqn.1$$

where U_{10} is wind speed at 10 m above the surface and U_2 is wind speed at 2 m above the surface.

Results

Air temperature

Air temperatures observed at each AWS and simulated by the WRF model with the 3DTKE and QNSE schemes are given in Fig. 2. Results for both tested horizontal resolutions (700 m and 300 m) are also presented. The leading multi-day temperature fluctuations were successfully captured by the model. Model accuracy was generally better from 25 May 2019 to 05 June 2019 while a positive bias prevailed from 06 – 12 June 2019.

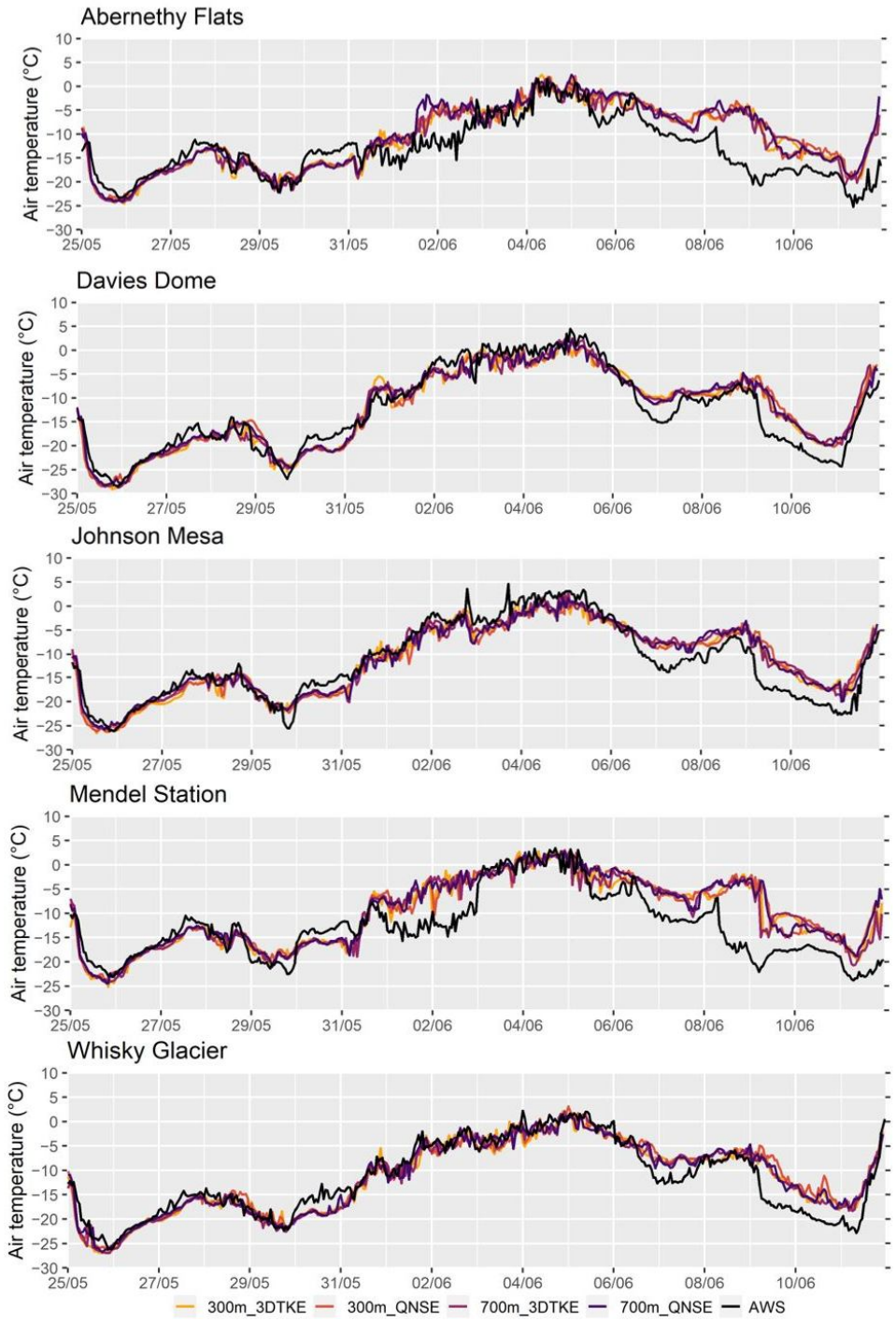

Fig. 2. Simulated and observed air temperatures at selected locations on Ulu Peninsula from 25 May 2019 01 UTC to 12 June 2019 00 UTC.

The model performed better in high-elevation sites (Davies Dome, Whisky Glacier, Johnson Mesa) with mean bias from 0.2°C to 0.6°C. The exact bias value depended on the model resolution and the selected PBL scheme, whose impact will be discussed in Chapter *Statistical evaluation of air temperature simulation*. The modelled temperature accuracy was lower at coastal (Mendel Station) or low-elevation (Abernethy Flats) sites where mean bias reached 2.0°C to 2.9°C. However, shorter-term biases showed significant variability, especially at low-elevation sites, where rather high bias was found during the 01 – 02 June 2019 and 06 – 11 June 2019 periods (Table 3). A common feature of these periods was strong temperature inversions, which occurred 01 – 02 June, 08 – 09 June and 11 June 2019.

AWS group	**25–31 May**	**01–02 June**	**03–05 June**	**06–11 June**
Low elevation	-1.2°C to -0.5°C	4.1°C to 7.5°C	0.3°C to 2.2°C	5.4°C to 6.5°C
High elevation	-1.4°C to -0.4°C	-1.6°C to -0.6°C	-2.5°C to -0.4°C	2.8°C to 3.8°C

Table 3. Mean WRF air temperature bias at low-elevation (Abernethy Flats, Mendel Station) and high-elevation (Davies Dome, Johnson Mesa, Whisky Glacier) locations during four validation subperiods. All the PBL scheme and resolution options are included in the intervals for each elevation zone of AWS and each study period.

Wind speed

The WRF model captured wind speed fluctuations very well (Fig. 3), with slightly positive bias at Davies Dome, a high-elevation AWS (1.3 $m \cdot s^{-1}$ to 1.6 $m \cdot s^{-1}$), and slight to moderate positive bias at Mendel Station (1.2 $m \cdot s^{-1}$ to 3.5 $m \cdot s^{-1}$), a low-elevation AWS. The impact of model setup on bias, which was more significant at Mendel Station that at Davies Dome, will be described in greater detail in Chapter *Statistical evaluation of wind speed simulation*. During air temperature inversion events, wind speed was overestimated at Mendel Station on 01 and 02 June 2019 (by values ranging from 2.2 $m \cdot s^{-1}$ to 4.2 $m \cdot s^{-1}$; Table 4) and 08 June 2019 (3.6 $m \cdot s^{-1}$ to 6.2 $m \cdot s^{-1}$) but only slightly on 11 June 2019 (0.2 $m \cdot s^{-1}$ to 1.7 $m \cdot s^{-1}$).

AWS	**25–31 May**	**01–02 June**	**03–05 June**	**06–11 June**
Mendel Station	0.5 $m \cdot s^{-1}$ to 3.8 $m \cdot s^{-1}$	2.2 $m \cdot s^{-1}$ to 4.2 $m \cdot s^{-1}$	3.2 $m \cdot s^{-1}$ to 4.5 $m \cdot s^{-1}$	0.7 $m \cdot s^{-1}$ to 2.6 $m \cdot s^{-1}$
Davies Dome	1.0 $m \cdot s^{-1}$ to 1.9 $m \cdot s^{-1}$	1.9 $m \cdot s^{-1}$ to 2.2 $m \cdot s^{-1}$	0.0 $m \cdot s^{-1}$ to 0.6 $m \cdot s^{-1}$	1.6 $m \cdot s^{-1}$ to 1.8 $m \cdot s^{-1}$

Table 4. Mean WRF wind speed bias at low-elevation Mendel Station and high-elevation Davies Dome for four validation subperiods. All the PBL scheme and resolution options are included in the intervals for each AWS and selected study period.

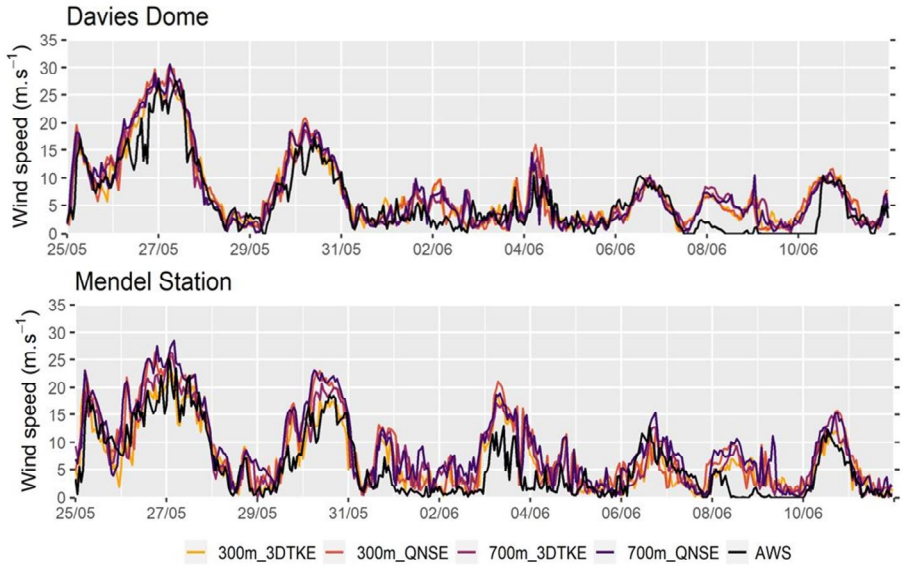

Fig. 3. Simulated and observed wind speeds at two selected locations on Ulu Peninsula from 25 May 2019 01 UTC to 12 June 2019 00 UTC.

Snow cover height and precipitation

There was no significant snowfall observed until 05 June 2019 – observed changes of < 1cm are within instrument error – but simulated snow cover reached 3 – 4 cm, of which the majority was related to the 26 – 27 May 2019 snowfall event. The most significant snowfall episode was recorded on 05 – 06 June 2019 with a maximum observed snow accumulation of 19 cm at both AWS locations. Modelled fresh snow height during this event reached 16 – 24 cm at Johnson Mesa AWS and 13 – 26 cm at Mendel Station AWS. The most accurate results were simulated with the 3D TKE scheme at 300 m (19.4 cm) at Mendel Station and with the QNSE scheme at 700 m (19.3 cm) at Johnson Mesa. Maximum snow height during the entire validation period was better simulated by both 300 m runs while the 700 m simulations produced snow cover that significantly exceeded the JUDD sonic ranger measurements. Observed snow height at Mendel Station showed a transient decrease around 07 June 2019 00 UTC and finally dropped off ~8 cm on 10 June 2019. On Johnson Mesa, almost all new snow accumulation was removed by wind by 07 June 2019 00 UTC. Note that during both 06 and 10 June 2019, maximum wind speeds at both Mendel Station and Davies Dome exceeded 10 m·s^{-1}.

Based on mean observed fresh snow density at Mendel Station and Whisky Glacier in summer 2022 (173.3 kg·m^{-3}), the amount of observed new snow on 05 – 06 June 2019 would correspond to 32.9 mm water equivalent. Modelled increase of SWE during these two days reached 19.7 – 20.6 mm for the 3D TKE and QNSE schemes at 300 m runs and 23.5 – 25.1 mm for the 700 m simulations (Table 5). The SWE of modelled fresh snow was very close to simulated precipitation amounts. A prevailing fraction of observed fresh snow accumulation was recorded on 06 June 2019

(64 – 81%), while the model simulated a bigger fraction during 05 June 2019 (52 – 75%); only the QNSE scheme on the 300 m grid setup lowered this fraction to 43%. Similar results were also found for SWE. The model thus predicted a large fraction of this snowfall event a few hours earlier than it was observed (*see* also Fig. 4).

Mendel Station	**Precipitation per 24 h (mm)**		**SWE (mm)**		**Snow height (cm)**	
	6.6.2019 00 UTC	7.6.2019 00 UTC	6.6.2019 00 UTC	7.6.2019 00 UTC	6.6.2019 00 UTC	7.6.2019 00 UTC
3D TKE 300 m	7.9	12.7	8.0	20.6	10.4	19.4
QNSE 300 m	7.4	12.3	7.4	19.7	5.8	13.4
3D TKE 700 m	11.8	13.0	11.8	24.8	16.4	26.4
QNSE 700 m	11.6	13.6	11.6	25.1	15.5	20.8
Observed	N/A	N/A	11.7	32.9	6.8	19.1
Johnson Mesa	**Precipitation per 24 h (mm)**		**SWE (mm)**		**Snow height (cm)**	
	6.6.2019 00 UTC	7.6.2019 00 UTC	6.6.2019 00 UTC	7.6.2019 00 UTC	6.6.2019 00 UTC	7.6.2019 00 UTC
3D TKE 300 m	8.6	11.4	8.7	20.1	10.1	17.3
QNSE 300 m	8.4	11.4	8.4	19.8	8.5	16.4
3D TKE 700 m	12.2	12.8	12.2	25.1	14.9	24.3
QNSE 700 m	11.9	11.6	11.9	23.5	12.3	19.3
Observed	N/A	N/A	6.4	32.9	3.7	19.3

Table 5. Modelled and observed precipitation amounts, snow water equivalent (SWE) and snow height for the 05 – 06 June 2019 snowfall event at Mendel Station and Johnson Mesa. Precipitation amount is given as a 24-hour sum (00 – 24 UTC). The SWE and snow height are accumulated from 05 June 2019 00 UTC, and their respective maximum values until 06 June 2019 00 UTC and 07 June 2019 00 UTC are shown. Maximum daily values are presented due to slightly different timing of modelled and observed peak snow heights. N/A = not available.

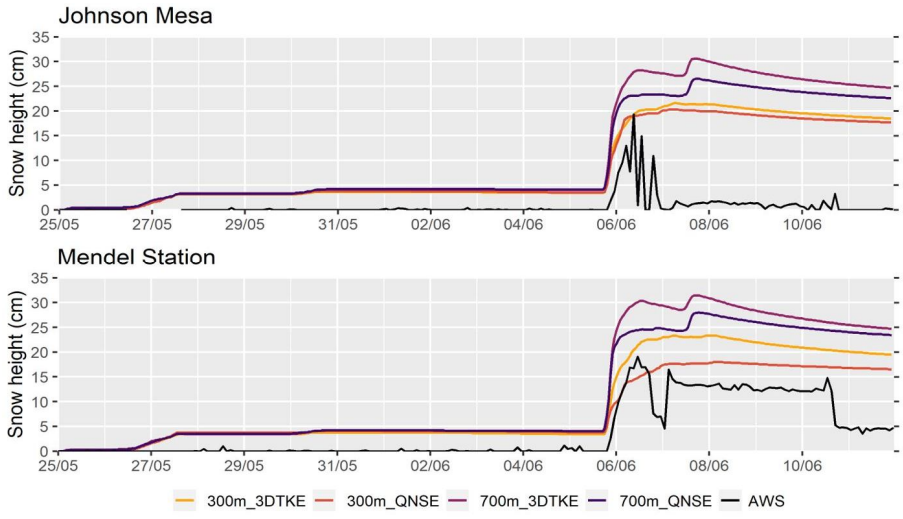

Fig. 4. Simulated and observed snow height at selected locations on Ulu Peninsula from 25 May 2019 01 UTC to 12 June 2019 00 UTC.

Statistical evaluation of air temperature simulation

Statistical parameters quantifying simulated air temperature accuracy are presented in Fig. 5. The model performed better at higher elevation sites – Davies Dome, Johnson Mesa and Whisky Glacier – with mean bias of 0.23 – 0.55°C, RMSE of 2.66 – 3.15°C and r_{xy} of 0.91 – 0.95. Model validation at coastal Mendel Station and low-elevation Abernethy Flats sites showed lower performance: bias of 2.01 – 2.91°C, RMSE of 4.39 – 5.37°C and r_{xy} of 0.79 – 0.81.

Selection of the new 3D TKE scheme led to an improvement in bias and RMSE at low-elevation AWS locations Mendel Station and Abernethy Flats. Compared with the QNSE runs at the same resolution, bias decreased by 0.29 – 0.56°C and RMSE by 0.16 – 0.44°C. At higher-elevation sites, the results are rather mixed. A slight improvement could be found at Whisky Glacier (bias improved by 0.10 – 0.32°C and RMSE by 0.07 – 0.36°C), whereas small changes at Davies Dome and Johnson Mesa were both positive and negative.

With increased horizontal model resolution (from 700 m to 300 m), bias was mostly reduced in the range of -0.27°C to +0.18°C, but RMSE increased in most cases (from -0.18°C to 0.42°C). Pearson correlation coefficients of modelled and observed air temperatures were within 0.01 range for any model setup at individual AWS locations. An exception was Whisky Glacier, where the QNSE-300 m run showed lower r_{xy} than other model setups by 0.02 – 0.03.

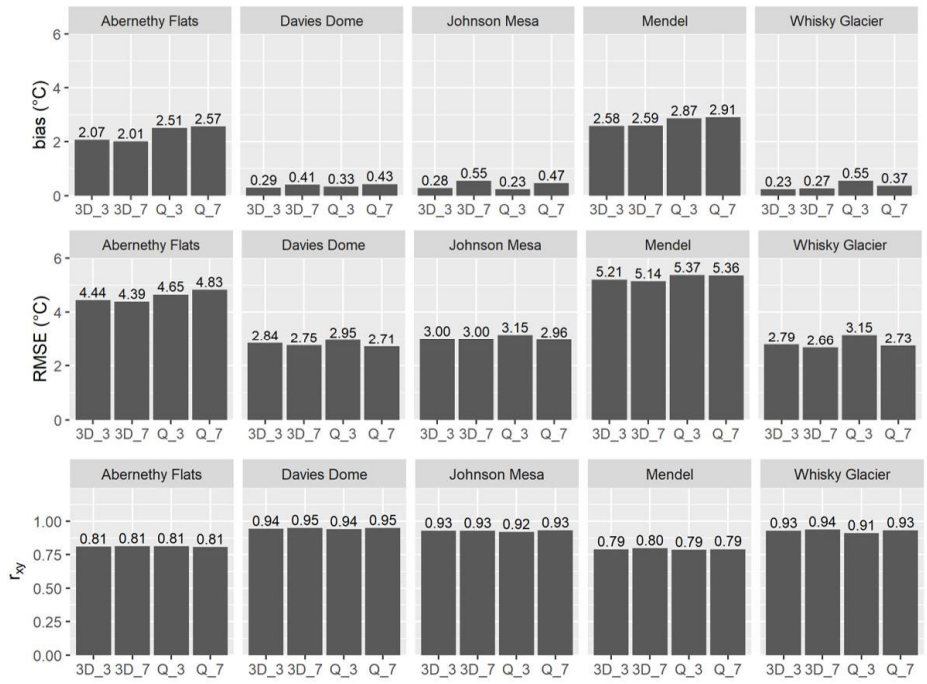

Fig. 5. Statistical evaluation of WRF-modelled air temperatures at selected Ulu Peninsula locations. Validation parameters are shown for 3D TKE and QNSE PBL schemes and for 700 m and 300 m model horizontal resolution. *Note*: 3D = 3D TKE, Q = QNSE, 3 = 300 m and 7 = 700 m.

Statistical evaluation of wind speed simulation

The WRF model with the 3D TKE scheme significantly reduced wind speed bias and RMSE at Mendel Station compared to the QNSE-based runs. The improvement reached 1.43 – 1.58 $m \cdot s^{-1}$ for bias and 0.99 – 1.05 $m \cdot s^{-1}$ for RMSE. Benefits of 0.03 – 0.36 $m \cdot s^{-1}$ in bias and 0.08 – 0.46 $m \cdot s^{-1}$ in RMSE were found for the 3D TKE simulations at Davies Dome. For the 3D TKE scheme, both bias and RMSE further improved when increasing model resolution from 700 m to 300 m. The same was true for the QNSE scheme at Mendel Station. However, increasing resolution of QNSE simulation did not lead to an improvement in RMSE at Davies Dome. Pearson correlation coefficients were within a 0.01 range for all model runs at Davies Dome but were 0.02 lower in the 3D TKE runs compared to the QNSE runs at Mendel Station.

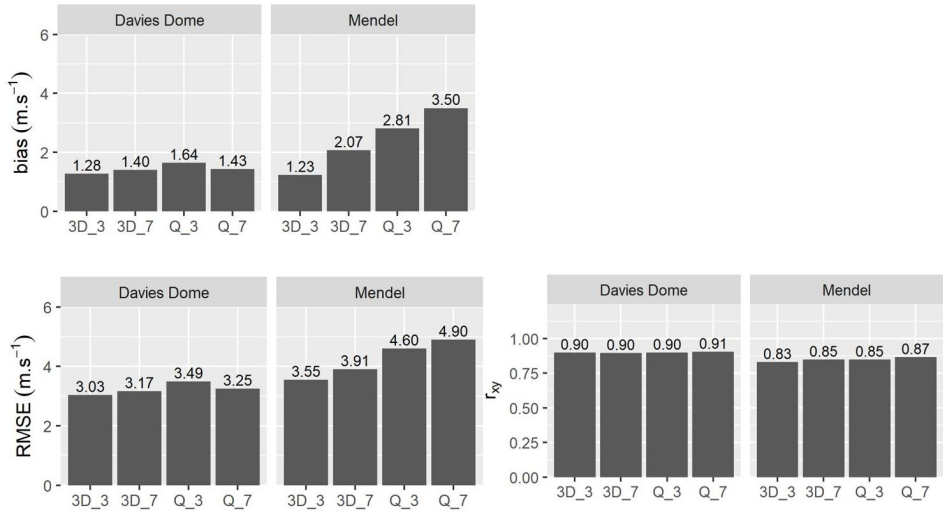

Fig. 6. Statistical evaluation of WRF-modelled wind speeds at selected Ulu Peninsula locations. Validation parameters are shown for 3D TKE and QNSE PBL schemes and for 700 m and 300 m model horizontal resolution. *Note*: 3D = 3D TKE, Q = QNSE, 3 = 300 m and 7 = 700 m.

Discussion

The WRF model simulated winter air temperatures and wind speeds during a selected period with different weather regimes on James Ross Island with very good accuracy. The model performance was similar or better to other Antarctic WRF validation studies (*e.g.* Turton et al. 2017, Deb et al. 2016). For a comprehensive summary of the WRF model validations in Antarctica, *see* Table 5 in Matějka et al. (2021).

At higher-elevation sites – Davies Dome, Whisky Glacier and Johnson Mesa (326 – 539 m a.s.l.) – the mean air temperature bias was 0.2 – 0.6°C for all PBL and horizontal resolution setups. A notable exception was 09 – 10 June 2019, when the model predicted ~5°C higher temperature

than observed values. Looking at low-elevation sites, the mean bias was higher (2.0 – 2.9°C), which may be attributed principally to three episodes of a strong temperature inversion: 01 – 02 June 2019, 08 – 09 June 2019 and 11 June 2019. It is clearly visible that the model performance was much better at high-elevated sites during these days. In fact, air temperature bias at the coastal Mendel Station was negatively correlated with a temperature difference between Mendel Station and Johnson Mesa (r_{xy} = -0.73; $p < 0.001$), that may be considered as a local air temperature lapse-rate proxy. Ambrožová et al. (2022) used the WRF model at 700 m horizontal resolution with the QNSE PBL scheme. They found almost no inversion in the model when comparing the Mendel Station and Bibby Hill (375 m a.s.l.) time series. However, it was realised that the inversion was simulated over sea ice in nearby Prince Gustav Channel. The suitability of the WRF model to simulate air temperature inversion in a less complex topography compared to northern James Ross Island was also confirmed over sea ice on the Weddell Sea (Tastula et al. 2012) and the Ross Ice Shelf (Wille et al. 2016). A possible explanation suggested by Ambrožová et al. (2022) is that, even at very high resolution, the numerical schemes in the model are not able to reproduce sharp temperature gradients at the foot of coastal hills. Based on this study, we suggest that increasing resolution further to 300 m is still not sufficient to accurately simulate very strong temperature stratification in the complex terrain of northern James Ross Island. However, using the 3D TKE scheme instead of the QNSE led to at least a slight improvement in air temperature bias at the low-elevation sites.

For wind speed, transition from the QNSE to the 3D TKE scheme and from 700 m to 300 m was highly beneficial at Mendel Station. At Davies Dome, the impact of model resolution was not entirely clear, but the combination of 3D TKE and 300 m produced the most accurate output from all model runs, similar to Mendel Station. Based on an analysis of wind speed and air temperature data, we suggest that exaggerated wind speed in the model contributed to a poor simulation of air temperature inversion at Mendel Station on 01 – 02 June 2019 and on 08 – 09 June 2019.

The main snowfall event during the study period occurred on 05 – 06 June 2019, when both AWS locations recorded 19 cm of new snow cover. The model estimated this amount and the timing of this event very well with a slight underestimation of fresh SWE. Snow transport by wind (5 – 10 $m \cdot s^{-1}$) led to snow height drops on 06 and 10 June 2019. Snowmelt in this period could be excluded due to sub-zero air temperature and negligible solar radiation. These snow height drops could not be simulated by the model because the NoahMP land surface scheme in the WRF model absents a blowing snow routine. Resultingly, there is a need for a snowdrift-permitting land surface model for reliable snow dynamics simulation on James Ross Island. Importance of snowdrift for glacier mass balance in this region was also emphasised by Engel et al. (2018).

Direct comparisons of WRF-modelled and observed snow heights in polar or subpolar regions are rare. Aas et al. (2016) used WRF-modelled meteorological data (*e.g.* air temperature and precipitation), as forcing for a glacier mass balance model on Svalbard and reached very good correspondence between observed and modelled mass balance. The WRF model was also proven to simulate spatial patterns of precipitation over Alaska and also, to a large extent, absolute precipitation values (Monaghan et al. 2018). These conclusions, together with this study's results, give good confidence to the WRF model's ability to predict snowfall with reasonable accuracy despite some differences in temporal distribution of observed and modelled snowfall (Fig. 4). However, a longer-period study of precipitation and snow height dy-

namics would be necessary to confirm model accuracy in the James Ross Island region. New precipitation and snow cover observations from summer 2021/2022 at Mendel Station might be very useful for this purpose in future WRF-based studies. Accurate precipitation prediction in polar regions with complex topography (*e.g.* northern AP) is crucial for subsequent glacier mass balance studies as well as for operational weather forecasts supporting field research activities.

Conclusion

In this study, new high-resolution WRF model output for James Ross Island is presented. The improvements from the new 3D TKE PBL scheme and enhanced horizontal model resolution for model performance were assessed. The most notable benefit of the new PBL scheme for air temperature simulation was reduction of bias and RMSE at low-elevation sites. However, all tested model configurations had difficulties in capturing strong low-level temperature inversions.

The new PBL scheme and better model resolution were beneficial for wind speed simulation at coastal Mendel Station, where the run with 300 m resolution with the 3D TKE scheme produced bias lower by 2.27 $m \cdot s^{-1}$ and RMSE lower by 1.35 $m \cdot s^{-1}$ than the 700 m run with the QNSE scheme. At Davies Dome, the best results were achieved also by the 300 m and 3D TKE combination, but the differences between schemes were less significant.

In addition to air temperature and wind speed, modelled snow cover heights at Mendel Station and Johnson Mesa were also evaluated. The WRF model captured the most important snowfall event of 05 – 06 June 2019 well, reaching similar fresh snow height as the observations showed. On the other hand, the model simulated another light snowfall event not found in observations. Finally, the need for a complex surface model with the ability to simulate snow transport by wind arose from analysis of snow height changes in this study.

We found that enhanced model resolution together with the 3D TKE PBL scheme have a profound effect on the WRF model's ability to simulate near-surface weather conditions in the AP region and James Ross Island in particular. With this WRF setup, the most significant improvements were found at low-elevation sites, where the model must deal with a complex topography and related meteorological phenomena (*e.g.* air temperature inversions and flow deformation by local orography). Increased model resolution also has a beneficial effect on modelled snow height, but further research is needed to assess the precipitation modelling skills of the WRF model in the AP region more thoroughly. For complex analyses of snow dynamics and glacier mass balance, we suggest use of the WRF model output as forcing of snow or hydrological models with included snowdrift capability, which is missing in standard WRF land surface schemes. These models include the Canadian Hydrological Model (Marsh et al. 2020) and the ALPINE3D model (Lehning et al. 2006).

References

AAS, K. S., BERNTSEN, T. K., BOIKE, J., ETZELMÜLLER, B., KRISTJÁNSSON, J. E., MATURILLI, M., SCHULER, T. V., STORDAL, F. and WESTERMANN, S. (2015): A comparison between simulated and observed surface energy balance at the Svalbard archipelago. *Journal of Applied Meteorology and Climatology*, 54: 1102-1119. doi: 10.1175/JAMC-D-14-0080.1

AAS, K.S., DUNSE, T., COLLIER, E., SCHULER, T.V., BERNTSEN, T.K., KOHLER, J. and LUKS, B. (2016): The climatic mass balance of Svalbard glaciers: A 1gree0-year simulation with a coupled atmosphere–glacier mass balance model. *The Cryosphere*, 10: 1089-1104. doi: 10.5194/tc-10-1089-2016

BINDSCHADLER, R., VORNBERGER, P., FLEMING, A., FOX, A., MULLINS, J., BINNIE, D., PAULSEN, S., GRANNEMAN, B. and GORODETZKY, D. (2008): The landsat image mosaic of Antarctica. *Remote Sensing of Environment*, 112: 4214-4226. doi: 10.1016/j.rse.2008.07.006

BROMWICH, D. H., OTIENO, F. O., HINES, K. M., MANNING, K. W. and SHILO, E. (2013): Comprehensive evaluation of polar weather research and forecasting model performance in the Antarctic. Polar weather research and forecasting model. *Journal of Geophysical Research*: *Atmospheres*, 118: 274-292. doi: 10.1029/2012JD018139

CAPE, M.R., VERNET, M., SKVARCA, P., MARINSEK, S., SCAMBOS, T. and DOMACK, E. (2015): Foehn winds link climate-driven warming to ice shelf evolution in Antarctica. *Journal of Geophysical Research*: *Atmospheres*, 120: 11,037-11,057. doi: 10.1002/2015JD023465

DAVIES, B. J., CARRIVICK, J. L., GLASSER, N. F., HAMBREY, M. J. and SMELLIE, J. L. (2012): Variable glacier response to atmospheric warming, northern Antarctic Peninsula, 1988–2009. *The Cryosphere*, 6: 1031-1048. doi: 10.5194/tc-6-1031-2012

DEB, P., ORR, A., HOSKING, J. S., PHILLIPS, T., TURNER, J., BANNISTER, D., POPE, J. O. and COLWELL, S. (2016): An assessment of the Polar Weather Research and Forecasting (WRF) model representation of near-surface meteorological variables over West Antarctica: Polar WRF Assessment Over West Antarctica. *Journal of Geophysical Research*: *Atmospheres*, 121: 1532-1548. doi: 10.1002/2015JD024037

ENGEL, Z., LÁSKA, K., NÝVLT, D. and STACHOŇ, Z. (2018): Surface mass balance of small glaciers on James Ross Island, north-eastern Antarctic Peninsula, during 2009–2015. *Journal of Glaciology*, 64: 349-361. doi: 10.1017/jog.2018.17

GALLÉE, H., TROUVILLIEZ, A., AGOSTA, C., GENTHON, C., FAVIER, V. and NAAIM-BOUVET, F. (2013): Transport of snow by the wind: A comparison between observations in Adélie Land, Antarctica, and simulations made with the regional climate model MAR. *Boundary-Layer Meteorology*, 146: 133-147. doi: 10.1007/s10546-012-9764-z

HERSBACH, H., BELL, B., BERRISFORD, P., HIRAHARA, S., HORÁNYI, A., MUÑOZ‐SABATER, J., NICOLAS, J., PEUBEY, C., RADU, R., SCHEPERS, D., SIMMONS, A., SOCI, C., ABDALLA, S., ABELLAN, X., BALSAMO, G., BECHTOLD, P., BIAVATI, G., BIDLOT, J., BONAVITA, M., CHIARA, G., DAHLGREN, P., DEE, D., DIAMANTAKIS, M., DRAGANI, R., FLEMMING, J., FORBES, R., FUENTES, M., GEER, A., HAIMBERGER, L., HEALY, S., HOGAN, R.J., HÓLM, E., JANISKOVÁ, M., KEELEY, S., LALOYAUX, P., LOPEZ, P., LUPU, C., RADNOTI, G., ROSNAY, P., ROZUM, I., VAMBORG, F., VILLAUME, S. and THÉPAUT, J. (2020): The ERA5 global reanalysis. *Quarterly Journal of the Royal Meteorological Society*, 146: 1999-2049. doi: 10.1002/qj.3803

HOWAT, I. M., PORTER, C., SMITH, B. E., NOH, M.-J. and MORIN, P. (2019): The reference elevation model of Antarctica. *The Cryosphere*, 13: 665-674. doi: 10.5194/tc-13-665-2019

IACONO, M. J., DELAMERE, J.S., MLAWER, E.J., SHEPHARD, M.W., CLOUGH, S.A. and COLLINS, W. D. (2008): Radiative forcing by long-lived greenhouse gases: Calculations with the AER radiative transfer models. *Journal of Geophysical Research*, 113: D13103. doi: 10.1029/2008JD009944

JOHNSON, H. K. (1999): Simple expressions for correcting wind speed data for elevation. *Coastal Engineering*, 36: 263-269. doi: 10.1016/S0378-3839(99)00016-2

JONSELL, U. Y., NAVARRO, F. J., BAÑÓN, M., LAPAZARAN, J. J. and OTERO, J. (2012): Sensitivity of a distributed temperature-radiation index melt model based on AWS observations and surface energy balance fluxes, Hurd Peninsula glaciers, Livingston Island, Antarctica. *The Cryosphere*, 6: 539-552. doi: 10.5194/tc-6-539-2012

KERN, S., OZSOY-ÇIÇEK, B. and WORBY, A. (2016): Antarctic sea-ice thickness retrieval from ICESat: Inter-comparison of different approaches. *Remote Sensing*, 8: 538. doi: 10.3390/rs8070538

LÁSKA, K., CHLÁDOVÁ, Z. and HOŠEK, J. (2017): High-resolution numerical simulation of summer wind field comparing WRF boundary-layer parametrizations over complex Arctic topography:

Case study from central Spitsbergen. *Meteorologische Zeitschrift*, 26: 391-408. doi: 10.1127/metz/2017/0796

LEHNING, M., VÖLKSCH, I., GUSTAFSSON, D., NGUYEN, T. A., STÄHLI, M. and ZAPPA, M. (2006): ALPINE3D: A detailed model of mountain surface processes and its application to snow hydrology. *Hydrological Processes*, 20: 2111-2128. doi: 10.1002/hyp.6204

MARSH, C. B., POMEROY, J. W. and WHEATER, H. S. (2020): The Canadian Hydrological Model (CHM) v1.0: A multi-scale, multi-extent, variable-complexity hydrological model – design and overview. *Geoscientific Model Development*, 13: 225-247. doi: 10.5194/gmd-13-225-2020

MATĚJKA, M., LÁSKA, K., JEKLOVÁ, K. and HOŠEK, J. (2021): High-resolution numerical modelling of near-surface atmospheric fields in the complex terrain of James Ross Island, Antarctic Peninsula. *Atmosphere*, 12: 360. doi: 10.3390/atmos12030360

MONAGHAN, A. J., CLARK, M. P., BARLAGE, M. P., NEWMAN, A. J., XUE, L., ARNOLD, J. R. and Rasmussen, R. M. (2018): High-resolution historical climate simulations over Alaska. *Journal of Applied Meteorology and Climatology*, 57: 709-731. doi: 10.1175/JAMC-D-17-0161.1

NIU, G.-Y., YANG, Z.-L., MITCHELL, K. E., CHEN, F., EK, M. B., BARLAGE, M., KUMAR, A., MANNING, K., NIYOGI, D., ROSERO, E., TEWARI, M. and XIA, Y. (2011): The community Noah land surface model with multiparameterization options (Noah-MP): 1. Model description and evaluation with local-scale measurements. *Journal of Geophysical Research*, 116: D12109. doi: 10.1029/2010JD015139

OLIVA, M., NAVARRO, F., HRBÁČEK, F., HERNÁNDEZ, A., NÝVLT, D., PEREIRA, P., RUIZ-FERNÁNDEZ, J. and TRIGO, R. (2017): Recent regional climate cooling on the Antarctic Peninsula and associated impacts on the cryosphere. *Science of The Total Environment*, 580: 210-223. doi: 10.1016/j.scitotenv.2016.12.030

SHIN, H. H., DUDHIA, J. (2016): Evaluation of PBL parameterizations in WRF at subkilometer grid spacings: Turbulence statistics in the dry convective boundary layer. *Monthly Weather Review*, 144: 1161-1177. doi: 10.1175/MWR-D-15-0208.1

SPREEN, G., KALESCHKE, L. and HEYGSTER, G. (2008): Sea ice remote sensing using AMSR-E 89-GHz channels. *Journal of Geophysical Research*, 113: C02S03. doi: 10.1029/2005JC003384

STEINHOFF, D. F., BROMWICH, D. H. and MONAGHAN, A. (2013): Dynamics of the foehn mechanism in the McMurdo Dry Valleys of Antarctica from polar WRF. *Quarterly Journal of the Royal Meteorological Society*, 139: 1615-1631. doi: 10.1002/qj.2038

SUKORIANSKY, S., GALPERIN, B. and PEROV, V. (2005): Application of a new spectral theory of stably stratified turbulence to the atmospheric boundary layer over sea ice. *Boundary-Layer Meteorology*, 117: 231-257. doi: 10.1007/s10546-004-6848-4

TASTULA, E.-M., VIHMA, T. (2011): WRF model experiments on the Antarctic atmosphere in winter. *Monthly Weather Review*, 139: 1279-1291. doi: 10.1175/2010MWR3478.1

TASTULA, E.-M., VIHMA, T. and ANDREAS, E. L. (2012): Evaluation of polar WRF from modeling the atmospheric boundary layer over Antarctic sea ice in autumn and winter. *Monthly Weather Review*, 140: 3919-3935. doi: 10.1175/MWR-D-12-00016.1

THOMPSON, G., FIELD, P. R., RASMUSSEN, R. M. and HALL, W. D. (2008): Explicit forecasts of winter precipitation using an improved bulk microphysics scheme. Part II: Implementation of a new snow parameterization. *Monthly Weather Review*, 136: 5095-5115. doi: 10.1175/2008MWR2387.1

TURNER, J., LU, H., WHITE, I., KING, J. C., PHILLIPS, T., HOSKING, J. S., BRACEGIRDLE, T. J., MARSHALL, G. J., MULVANEY, R. and DEB, P. (2016): Absence of 21st century warming on Antarctic Peninsula consistent with natural variability. *Nature*, 535: 411-415. doi: 10.1038/nature18645

TURTON, J. V., KIRCHGAESSNER, A., ROSS, A. N. and KING, J. C. (2017): Does high-resolution modelling improve the spatial analysis of föhn flow over the Larsen C Ice Shelf? *Weather*, 72: 192-196. doi: 10.1002/wea.3028

TURTON, J.V., MÖLG, T. and VAN AS, D. (2019): Atmospheric processes and climatological characteristics of the 79N Glacier (Northeast Greenland). *Monthly Weather Review*, 147: 1375-1394. doi: 10.1175/MWR-D-18-0366.1

WANG, W., BRUYERE, C., DUDA, M., DUDHIA, J., GILL, D., KAVULICH M., WERNER, K., CHEN, M., LIN, H-CH., MICHALAKES, J., RIZVI, S., ZHANG X., BERNER, J., MUNOZ-ESPARZA, D., REEN, B., HA, S. and FOSSELL, K. (2021): User's guide for the advanced research WRF (ARW) modeling system version 4.3. *Available at*: https://www2.mmm.ucar.edu/wrf/users/docs/user_guide_v4/v4.3/contents.html

WILLE, J. D., BROMWICH, D. H., CASSANO, J. J., NIGRO, M. A., MATELING, M. E. and LAZZARA, M. A. (2017): Evaluation of the AMPS boundary layer simulations on the Ross ice shelf, Antarctica, with Unmanned Aircraft Observations. *Journal of Applied Meteorology and Climatology*, 56: 2239-2258. doi: 10.1175/JAMC-D-16-0339.1

WARNER, T. T. (2011): Numerical weather and climate prediction. Cambridge University Press, Cambridge, New York, 526 p.

ZHANG, X., BAO, J.-W., CHEN, B. and GRELL, E. D. (2018): A three-dimensional scale-adaptive turbulent kinetic energy scheme in the WRF-ARW model. *Monthly Weather Review*, 146: 2023-2045. doi: 10.1175/MWR-D-17-0356.1

ZHANG, C., ZHANG, J. (2018): Modeling study of foehn wind events in Antarctic Peninsula with WRF Forced by CCSM. *Journal of Meteorological Research*, 32: 909-922. doi: 10.1007/s13351-018-8067-9

Web sources / Other sources

[1] Antarctic Mesoscale Prediction System
https://www2.mmm.ucar.edu/rt/amps/

[2] British Antarctic Survey: SCAR Antarctic Digital Database (2019): *Available online*: https://add.data.bas.ac.uk/repository/entry/show?entryid=f477219b-9121-44d6-afa6-d8552762dc45 (accessed on 14 October 2018).

[3] Czech Geological Survey (2009): James Ross Island—Northern part. Topographic Map 1: 25 000, Czech Geological Survey: Prague. ISBN 978-80-7075-734-5.

[4] IPCC (2019): The ocean and cryosphere in a changing climate: Special report of the Intergovernmental Panel on Climate Change, 1st ed. Cambridge University Press. https://doi.org/ 10.1017/9781009157964